PLANETARY SCIENCE

Imprint of chondrule formation on the K and Rb isotopic compositions of carbonaceous meteorites

Nicole X. Nie[1,2]*, Xin-Yang Chen[3], Timo Hopp[1], Justin Y. Hu[1], Zhe J. Zhang[1], Fang-Zhen Teng[3], Anat Shahar[2], Nicolas Dauphas[1]

Chondrites display isotopic variations for moderately volatile elements, the origin of which is uncertain and could have involved evaporation/condensation processes in the protoplanetary disk, incomplete mixing of the products of stellar nucleosynthesis, or aqueous alteration on parent bodies. Here, we report high-precision K and Rb isotopic data of carbonaceous chondrites, providing new insights into the cause of these isotopic variations. We find that the K and Rb isotopic compositions of carbonaceous chondrites correlate with their abundance depletions, the fractions of matrix material, and previously measured Te and Zn isotopic compositions. These correlations are best explained by the variable contribution of chondrules that experienced incomplete condensation from a supersaturated medium. From the data, we calculate an average chondrule cooling rate of ~560 ± 180 K/hour, which agrees with values constrained from chondrule textures and could be produced in shocks induced by nebular gravitational instability or motion of large planetesimals through the nebula.

INTRODUCTION

Chondrites are primitive meteorites that formed 2 to 3 million years after the birth of the solar system (*1*) and may represent the building blocks of the terrestrial planets (*2*, *3*). Many of these meteorites show variable depletions in moderately volatile elements (MVEs) that were presumably produced by evaporation and condensation processes (*4*). Isotopic analyses can potentially shed light on these processes because isotopic ratios are sensitive to the mechanisms (evaporation or condensation) and conditions (degrees of undersaturation or supersaturation) associated with volatile element loss (*5*–*8*). Alkali elements have been the focus of many studies because they present a large range of volatility (from refractory Li to highly volatile Cs) (*9*), and the isotopic compositions of some of them (Li, K, and Rb) can be measured precisely with modern instrumentation (*10*). They are also strongly lithophile, meaning that interpretations are not obscured by metal or sulfide separation in the nebula or planetary cores.

Because of its high abundance, K has been the focus of several recent isotopic studies that tried to understand the reason why MVEs are depleted in planetary bodies (*11*–*16*). Alexander *et al.* (*11*, *12*) studied the isotopic compositions of K in single chondrules using in situ secondary ion mass spectrometry (SIMS) and found limited K isotopic fractionation, implying that during chondrule formation, K was evaporated in a nearly saturated vapor medium. Bloom *et al.* (*16*) studied K isotopic compositions of various bulk chondrite samples and suggested that K isotopic variations in chondrites were mainly controlled by condensation and vaporization processes, but the physicochemical conditions remained unclear. Wang and Jacobsen (*13*), Tian *et al.* (*15*), Pringle and Moynier (*17*), and Nie and Dauphas (*18*) reported heavy K and Rb isotopic compositions in lunar rocks compared with Earth. Nie and Dauphas (*18*) showed that these heavy isotope enrichments in the Moon were consistent with evaporation in a vapor medium that was 99% saturated, consistent with a scenario involving loss of MVEs in the aftermath of the giant impact by viscous drainage of vapor in the protolunar disk onto Earth. All these studies assumed that K and Rb isotopic variations were produced by high-temperature evaporation and condensation processes, as well as mixing of variably depleted components. More recent studies have challenged this interpretation and suggested instead that K isotopic variations in planetary bodies could be due to (i) the presence of nucleosynthetic anomalies produced by heterogeneous distribution of the products of stellar nucleosynthesis in the protoplanetary disk (*19*) or (ii) alkali element mobility associated with parent body aqueous alteration (*20*–*22*).

The isotopic compositions of MVEs Te, Zn, and Rb seem to correlate with their depletions in carbonaceous chondrites (CCs), which was interpreted to reflect mixing between nebular components (most likely matrix and chondrules) (*17*, *23*–*26*). However, the origin of the mixing endmembers remains debated. The isotopic compositions of these elements and K have also shown to be correlated with isotopic anomalies of ^{17}O and ^{54}Cr (*17*, *19*, *23*–*25*). Tellurium and zinc isotopic variations are clearly mass dependent, but one cannot tell from the two isotopes measured for either K (^{41}K and ^{39}K; low-abundance ^{40}K is usually not analyzed) or Rb (^{87}Rb and ^{85}Rb) whether the isotopic variations reflect inheritance of nucleosynthetic anomalies or mass-dependent fractionation associated with evaporation/condensation. Here, we report coupled Rb and K isotopic analyses of bulk CCs to elucidate the origin of K and Rb isotopic variations in those meteorites. Given that K and Rb have similar geochemical behaviors, evaporation and condensation would produce correlated isotopic variations for the two elements, which would not be expected for presolar nucleosynthetic heterogeneity given that the two elements are synthesized at different sites in stars (*27*, *28*).

RESULTS

Bulk CCs were measured for their Rb and K isotopic compositions. Given that Rb and K are fluid mobile and can be contaminated during residence at Earth's surface (*14*, *19*), the samples studied here are limited to meteorite falls. Meteorite falls can still be

[1]Origins Laboratory, Department of the Geophysical Sciences and Enrico Fermi Institute, The University of Chicago, Chicago, IL 60637, USA. [2]Earth and Planets Laboratory, Carnegie Institution for Science, Washington, DC 20015, USA. [3]Isotope Laboratory, Department of Earth and Space Sciences, University of Washington, Seattle, WA 98195, USA.
*Corresponding author. Email: nnie@carnegiescience.edu

contaminated (*19*) between fall and recovery or during handling and storage, but the likelihood of contamination is much lower than for finds. The samples measured (Table 1) belong to four main CC groups (CI, CM, CV, and CO) and comprise eight meteorites. Samples were obtained in either powder form (>500 mg each) or as rock chips. Rock chips weighing more than 300 mg were powdered in a precleaned agate mortar. Aliquots of homogenized powders weighing 90 to 120 mg were transferred into fluoropolymer beakers, digested in various mixtures of HF-HNO_3-HCl-$HClO_4$ acids, and then purified for Rb and K isotopic analyses (see Materials and Methods). Purified Rb was measured for its isotopic composition using a ThermoFinnigan Neptune multicollector-inductively coupled plasma mass spectrometer (MC-ICPMS) at the University of Chicago (*18*), while K was measured using a Nu Plasma II MC-ICPMS at the University of Washington (*29*). The isotopic compositions are expressed in δ^{87}Rb and δ^{41}K notations, which are per mil (‰) departures of the $^{87}Rb/^{85}Rb$ and $^{41}K/^{39}K$ ratios relative to the reference material SRM984 and SRM3141a, respectively. Uncertainties are reported as 95% confidence intervals (c.i.) of 5 to 12 repeat analyses for each sample.

The Rb and K isotopic compositions of the measured CCs are reported in Table 1. For Rb, the data overlap with previous data (*17*), but some discrepancies are present (fig. S1). To test the accuracy of our Rb isotopic results, we treated selected samples (Allende and Murchison) using two different chromatographic methods to purify Rb, and we obtained consistent results (see the evaluation of data accuracy in Materials and Methods). Measurements of CI chondrites reveal large K isotopic variations well beyond analytical uncertainties (ranging from −0.04 to −0.46‰ for Orgueil and Ivuna; from light to terrestrial-like values), while samples in other groups are less scattered (Table 1) (*19*). Large variations have been documented previously for Te isotopes between different aliquots of the Orgueil meteorite (*30*). For K isotopes, the dispersion in CI chondrites could be due to (i) K redistribution and isotopic fractionation by aqueous alteration on the parent body (*20*–*22*) and unrepresentative sampling or to (ii) terrestrial contamination during sample handling since collection (*19*). The first explanation would mean that the mean K isotopic composition of CI is poorly known and further work is needed to better define it. The second interpretation would mean that the CI samples with terrestrial-like composition should be excluded, as was suggested by Ku and Jacobsen (*19*). At the present time, we cannot tell which interpretation is correct. Nonetheless, the δ^{41}K value of Ivuna appears to be an outlier in several of our plots (Figs. 1 to 3), and given its near-terrestrial composition, we have decided to follow (*19*) and exclude it from further consideration.

We find statistically significant linear correlations between the isotopic compositions of MVEs Rb, K, Te (*23*), and Zn (*24*, *25*) in bulk CCs (Fig. 1). The isotopic correlations between Rb, Te, and Zn are very well defined, while that between Rb and K shows more scatter. The scatter thus is most likely due to variations in K isotopic composition, which also has larger analytical uncertainty. Large K

Table 1. Rubidium and potassium concentrations and isotopic compositions of carbonaceous chondrites. δ^{87}Rb and δ^{41}K are isotopic ratio deviations in per mil relative to reference materials NIST SRM984 and SRM3141a, respectively.

Sample	Type	Fall/find	Dissolved mass (mg)	δ^{87}Rb (‰)	95% c.i.	δ^{41}K (‰)	95% c.i.	K (μg/g)	Rb (μg/g)
Carbonaceous chondrites									
Orgueil*	CI1	Fall	91.3	0.194	0.034	−0.039	0.038	390.9	1.9
Orgueil†	CI1	Fall	101.6	0.159	0.042	−0.144	0.059	490.6	2.1
Ivuna	CI1	Fall	99.6	0.131	0.042	−0.460	0.046	457.5	1.8
Murchison	CM2	Fall	90.7	0.119	0.024	−0.101	0.034	320.3	1.5
Murchison‡	CM2	Fall	96.3	0.099	0.023				
Mighei	CM2	Fall	91.5	0.126	0.032	−0.158	0.046	394.3	1.5
Allende	CV3	Fall	118.9	0.091	0.024	−0.201	0.038	256.2	1.1
Allende‡	CV3	Fall	103.4	0.069	0.034				
Allende‡	CV3	Fall	100.0	0.087	0.030				
Vigarano	CV3	Fall	97.0	0.057	0.020	−0.346	0.038	269.8	1.0
Ornans	CO3.4	Fall	99.4	0.100	0.024	−0.046	0.038	344.7	1.3
Lancé	CO3.5	Fall	107.0	0.029	0.030	−0.235	0.034	346.0	1.0
Terrestrial geostandards									
BCR-2	Basalt		52.6	−0.169	0.029	−0.423	0.037		
BHVO-2	Basalt		104.9	−0.117	0.014	−0.391	0.078		
AGV-2	Andesite		103.6	−0.154	0.014	−0.462	0.044		
G-3	Granite		17.6	−0.229	0.020	−0.439	0.033		

*,†Powders from different fragments. ‡Rubidium was separated using a different column chromatography method devised to test the accuracy of the Rb isotopic data (see Materials and Methods).

isotopic variations within each CC subgroup have been observed in previous studies (*16*, *19*), and no clear correlation between K isotopic variations with geochemical indicators (e.g., degree of depletion, petrological types, weathering index, and degree of shock metamorphism) was found (*16*). The reason for the slightly different behavior of K compared to Rb, Zn, and Te is unclear but could be due to the fact that K is less volatile (*9*) or that it is more fluid mobile and experienced extensive aqueous alteration on the parent bodies (*20*–*22*). Similar to what was suggested previously for Te and Zn (*23*–*26*), we find statistically significant correlations between (i) the Rb, K, Zn, and Te concentrations and the mass fractions of matrix (*23*, *26*) in the CC groups (Fig. 2, A to D), as well as (ii) the isotopic compositions of Rb, K, Zn, and Te and their respective concentrations in the CC bulk samples (Fig. 2, E to H).

DISCUSSION

Mixing between chondrules and matrix modulates MVE abundances and isotopic compositions in CCs

Chondrites represent complex mixtures between components formed at different stages and in different environments, notably chondrules (quenched silicate spherules), matrix (fine-grained interstitial material rich in silicates, metal, water, organics, and presolar grains), and refractory inclusions (high-temperature condensates and evaporation residues). Refractory inclusions were formed at high temperature and are dominated by refractory elements. The MVEs that can now be found in them are thought to be of secondary origin, meaning that they were introduced by fluid circulation and metamorphism during parent body alteration [e.g., (*31*, *32*)]. Therefore, the two main components that control the mass balance of MVEs in

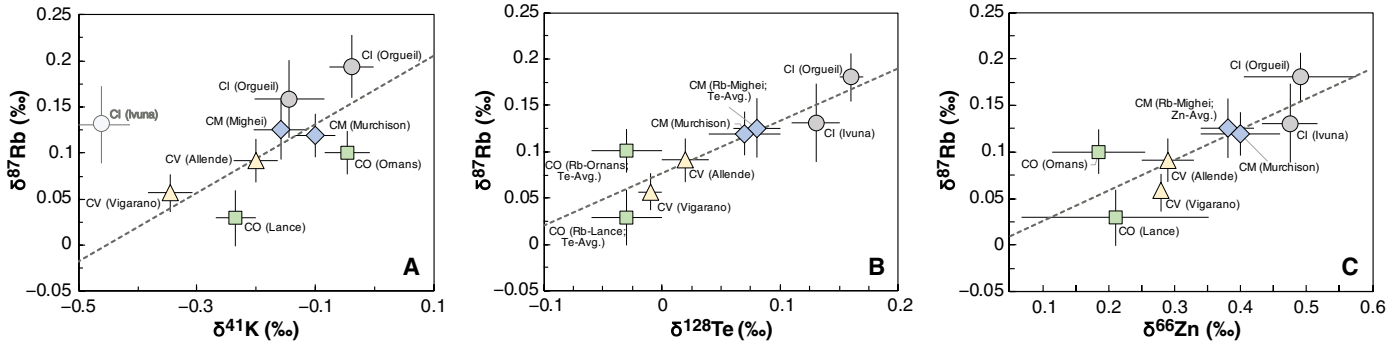

Fig. 1. Correlations between the isotopic compositions of Rb, K, Te, and Zn in bulk CCs. The Rb and K data are from this study (Table 1), and the Te and Zn data are from (*23*–*25*). Group average (Avg.) is used when data are not available for an individual sample. The correlations between δ^{87}Rb, δ^{128}Te, and δ^{66}Zn (**B** and **C**) are well defined, while δ^{87}Rb versus δ^{41}K (**A**) shows more scatter. One of the CI chondrites, Ivuna [unfilled circle in (A)], has terrestrial-like K isotopic composition and plots off the trend. It is also an outlier when plotting K isotopic composition versus elemental concentration (see Fig. 2).

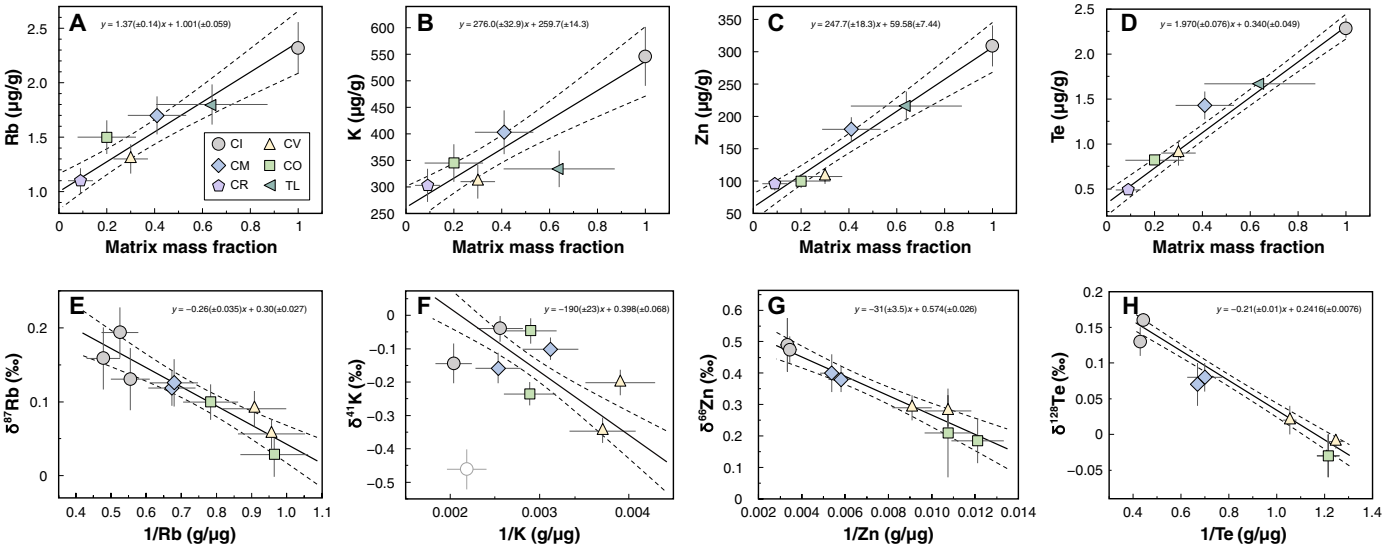

Fig. 2. Correlations between MVE elemental abundances, isotopic compositions, and mass fractions of matrix material in CCs. Correlations are observed between MVE elemental abundances and matrix mass fractions in CC groups (**A** to **D**; top) and between isotopic compositions and inverse of elemental concentrations in bulk CC samples (**E** to **H**; bottom). The correlations can be explained by binary mixing between a CI-like matrix and a chondrule component. The correlations were used to calculate the elemental concentration and isotopic composition of the chondrule and matrix components [see "Mixing between chondrules and matrix modulates MVE abundances and isotopic compositions in CCs" (Discussion) and table S1]. For (A) to (D), the matrix mass fractions, Te concentrations, and their uncertainties are from (*23*). Concentrations of Rb, K, and Zn in CC groups are from (*26*), and a ±10% error was assigned to them. For (E) to (H), Rb and K elemental concentrations and isotopic compositions are from this study (Table 1). Zn and Te concentrations and isotopic compositions are from (*23*–*25*). The unfilled circle in (F) represents the outlier Ivuna.

CCs are the matrix and chondrules. As proposed previously in (*26*, *33*, *34*) to explain the elemental abundance patterns and as discussed by Hellmann *et al.* (*23*) for Te isotopes and by Luck *et al.* (*24*) and Pringle *et al.* (*25*) for Zn isotopes, the presence of matrix and chondrules in varying proportions is the most likely reason why bulk CCs define binary mixing lines in chemical and isotopic diagrams (Figs. 2 and 3). Ordinary and enstatite chondrites (NCs) show more complex behaviors presumably because they contain other extraneous components such as alkali-rich clasts in ordinary chondrites [e.g., (*35*, *36*)] and sulfide minerals (including K,Rb-sulfide Djerfisherite) in enstatite chondrites (*37*), which can contribute to the bulk inventory of MVEs. Many NC samples have also experienced higher grades of thermal metamorphism than CCs, which can modify the isotopic compositions of MVEs, as observed for Te, Cd, and Ag (*30*, *38*–*40*).

The reason for the spread in MVE inventories and isotopic compositions among CC meteorites (Figs. 1 to 3) is that the proportions of matrix and chondrules differ in each CC subgroup (*23*–*26*). The matrix content is constrained to be approximately 100 weight % (wt %) in CI, 41 ± 12 wt % in CM, 30 ± 7 wt % in CV, 20 ± 12 wt % in CO, 9 ± 5 wt % in CR, and 64 ± 23 wt % in Tagish Lake (TL) (*23*, *26*). Assuming two-component chondrule-matrix mixing for MVEs, we can calculate the elemental and isotopic compositions of the chondrule reservoir (referred to as the "chondrule component" hereafter). Following Hellman *et al.* (*23*), we first use the correlation between elemental concentration and matrix mass fraction (the two should be linearly correlated during mixing) (Fig. 2, A to D) to calculate the elemental concentration at a matrix mass fraction of zero, which represents the elemental concentration in the chondrule component. To precisely constrain the isotopic composition, we extrapolate the mixing relationships between δ values and the reciprocals of the elemental concentrations in Fig. 2 (E to H) to the concentrations of the chondrule component calculated using Fig. 2 (A to D). The calculated elemental compositions of the chondrule component are [Rb] = 1.00 ± 0.06 μg/g, [K] = 260 ± 14 μg/g, [Te] = 0.34 ± 0.05 μg/g, and [Zn] = 60 ± 7 μg/g (table S1). The calculated isotopic compositions of the chondrule component are δ^{87}Rb = +0.04 ± 0.05‰, δ^{41}K = −0.33 ± 0.12‰, δ^{128}Te = −0.38 ± 0.09‰, and δ^{66}Zn = +0.05 ± 0.09‰ (table S1). We can also calculate the isotopic compositions of the CI-like matrix using the linear relationships in Fig. 2 (E to H) by extrapolating the linear relationships to the elemental concentrations of the matrix ([Rb] = 2.4 ± 0.2 μg/g, [K] = 536 ± 36 μg/g, [Te] = 2.3 ± 0.1 μg/g, and [Zn] = 307 ± 20 μg/g; table S1), and the calculated isotopic compositions are δ^{87}Rb = +0.19 ± 0.03‰, δ^{41}K = +0.04 ± 0.08‰, δ^{128}Te = +0.15 ± 0.01‰, and δ^{66}Zn = +0.47 ± 0.03‰ (table S1). The isotopic compositions of the matrix calculated in this manner are the same as the measured values of CI chondrites within error (table S1). This binary mixing model assumes that the matrix component is the

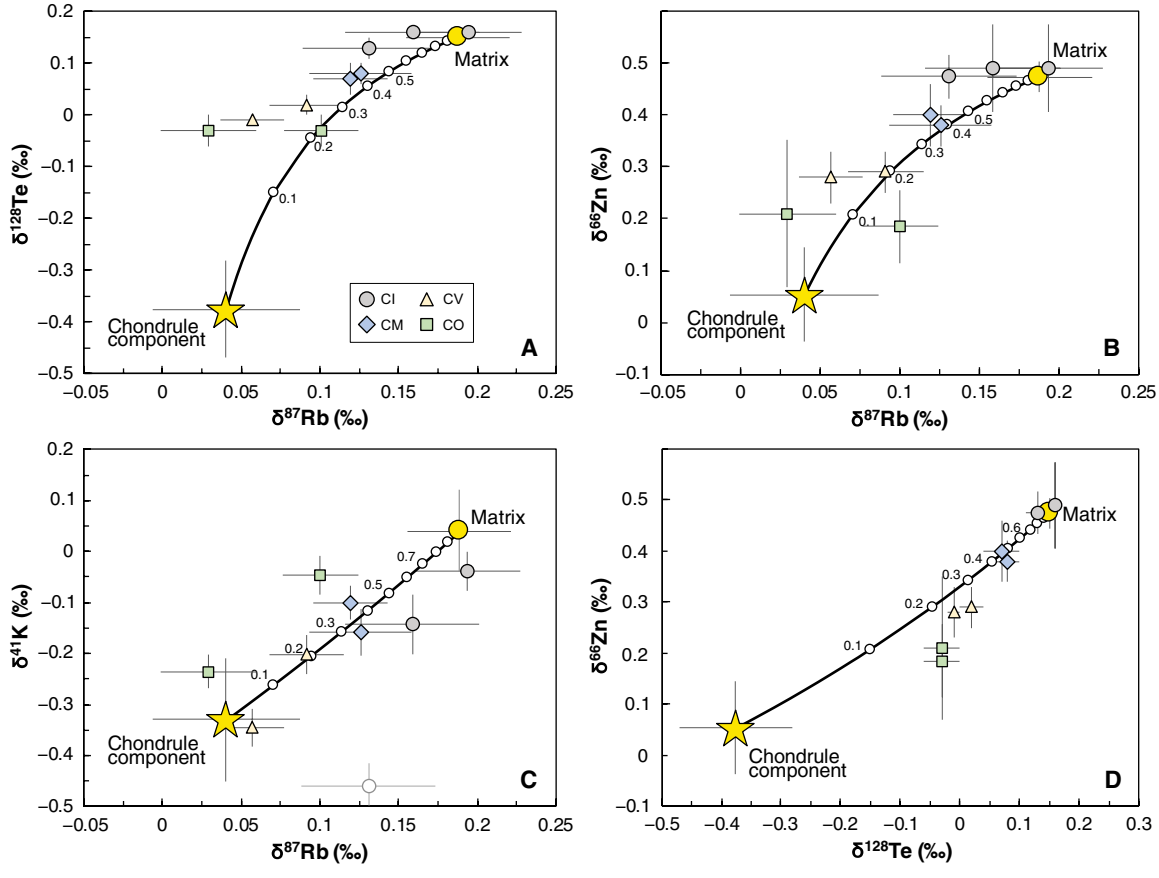

Fig. 3. Mixing between the chondrule component and CI-like matrix can explain the observed isotopic correlations of MVEs in CCs. The plots show mixing between isotopes of Te and Rb (**A**), Zn and Rb (**B**), K and Rb (**C**), and Zn and Te (**D**). The mass fractions of matrix (small unfilled circles) in the chondrule-matrix mixture are indicated on the modeled mixing curves (black lines).

same for all chondrites, an approach that has been used previously to explain chemical and isotopic variations among CCs (*23*, *26*, *33*, *34*). In reality, the measured major element compositions of the matrix (e.g., Si/Mg ratios and Fe/Mg ratios) vary among CC meteorites (*41*, *42*), but much of this variation could reflect redistribution of elements between chondrules and matrix by aqueous alteration and thermal metamorphism (*43*, *44*). Our finding that the isotopic compositions of MVEs can be explained by mixing between the two components is consistent with this view.

We are primarily interested in the degree to which MVEs in the chondrule component are depleted and isotopically fractionated relative to the matrix (CI) composition, which represents the composition of the chondrule precursor. The elemental abundances of the chondrule component relative to matrix are [Rb] = 0.42 ± 0.04 CI, [K] = 0.48 ± 0.04 CI, [Te] = 0.15 ± 0.02 CI, and [Zn] = 0.19 ± 0.03 CI (table S1). The isotopic fractionations of the chondrule component relative to the matrix are Δ^{87}Rb = −0.15 ± 0.06‰, Δ^{41}K = −0.37 ± 0.15‰, Δ^{128}Te = −0.53 ± 0.10‰, and Δ^{66}Zn = −0.42 ± 0.10‰ (table S1). The concentrations calculated for the chondrule component are lower than the CI-like matrix, consistent with the fact that chondrules were formed at high temperature and were depleted in MVEs. The chondrule component has lighter isotopic compositions than the matrix, consistent with previous bulk chondrule measurements (*22*, *25*, *45*). As discussed below, the finding that chondrules have, on average, light isotopic compositions not only for Te and Zn but also for K and Rb is important as it puts new constraints on the thermal history of chondrules.

Our approach of relying on bulk measurements of CCs to infer the average composition of chondrules by extrapolating binary mixing relationships to a null matrix fraction overcomes difficulties that have plagued analyses of single chondrules by either in situ SIMS (*11*, *12*) or wet chemistry MC-ICPMS (*20*, *22*). A critical one is that most chondrules have been altered and have exchanged with the matrix during parent body alteration/metamorphism [e.g., (*20*, *22*, *31*)]. Our approach is insensitive to the redistribution of MVEs between matrix and chondrules by chondrite parent body processes, as long as these processes did not redistribute MVEs at the bulk sample scale.

Condensation as the main driver of MVE depletion and isotopic fractionation in chondrules

As discussed above, the chondrule component is depleted in volatile elements Rb, K, Te, and Zn and has lighter isotopic composition than the matrix (CI). Previous Zn isotope measurements of chondrules from Allende, Mokoia, and Leoville CV chondrites revealed light Zn isotope enrichments in chondrules, which were interpreted to reflect removal of isotopically heavy sulfide from chondrules or their precursors (*25*, *45*). This interpretation might also be able to explain the light Te isotopic composition of the chondrule component because chalcophile Te can partition into sulfides. However, this scenario cannot explain the light Rb and K isotopic compositions reported here because these two elements are strongly lithophile and do not partition into metals or sulfides.

Ku and Jacobsen (*19*) argued that K isotopic variations in chondrites reflected isotopic anomalies (i.e., mass-independent isotopic fractionations) that were produced by incomplete mixing of products of nucleosynthesis. We find, however, that the isotopic compositions of the MVEs K, Rb, Zn, and Te correlate, and all point to a reservoir (chondrules) that, on average, is characterized by light isotopic compositions. Among the four elements, Zn and Te have sufficient measurable isotopes to detect anomalies, and the isotopic variations are clearly mass dependent (*23*–*25*). The correlation between δ^{87}Rb and δ^{41}K in CC meteorites has a slope of ~0.38 ± 0.29 (excluding Ivuna; Fig. 1) that is close to the slope associated with isotopic fractionation during evaporation and condensation processes (the theoretical kinetic slope is $\ln\frac{m(^{85}\mathrm{Rb})}{m(^{87}\mathrm{Rb})}/\ln\frac{m(^{39}\mathrm{K})}{m(^{41}\mathrm{K})} = 0.46$, and the theoretical equilibrium slope is $\frac{1/m(^{85}\mathrm{Rb})-1/m(^{87}\mathrm{Rb})}{1/m(^{39}\mathrm{K})-1/m(^{41}\mathrm{K})} = 0.22$), while no correlation would be expected for nucleosynthetic anomalies given that K and Rb are produced by different nucleosynthetic processes at different stellar sites. Specifically, ^{39}K and ^{41}K are both produced by oxygen burning in core-collapse supernovae, while ^{85}Rb is produced mainly by the r-process in core-collapse supernovae and neutron star mergers, and ^{87}Rb is produced mainly by the s-process in asymptotic giant branch stars (*27*, *28*). Ku and Jacobsen (*19*) used the trends between K isotopic ratios and nucleosynthetic ^{54}Cr and ^{64}Ni anomalies to argue for a nucleosynthetic origin of K isotopic variation. However, similar trends have been observed in CCs between mass-dependent Zn and Te isotopic fractionations on the one hand, and mass-independent ^{17}O and ^{54}Cr anomalies on the other hand (*23*–*25*). These correlations indicate that chondrules likely received a slightly different nucleosynthetic heritage than the matrix (*23*–*25*). Therefore, the correlations between K isotopes and mass-independent ^{54}Cr and ^{64}Ni anomalies in bulk CCs merely reflect chondrule-matrix mixing. We conclude that the isotopic variations of K and Rb in CCs, likely also other MVEs, are produced by fractionation during evaporation/condensation associated with chondrule formation, and a nucleosynthetic origin for K isotopic variation is highly implausible.

Distinguishing between equilibrium and kinetically controlled evaporation/condensation processes is important because melt-gas interactions are thought to play a major role in the evolution of chondrule mineralogy and chemistry (*46*, *47*). Measurements of Na in chondrule olivine phenocrysts and their melt inclusions have shown that even at near-peak temperature when olivine was crystalizing, large amount of Na remained in the melt (*48*–*50*). This indicates that the gas pressure around chondrules was sufficient for Na vapor pressure to build up to near equilibrium, limiting the extent of Na loss even at high temperature (*48*–*52*). The K isotopic compositions of individual chondrules show subdued isotopic fractionation relative to expectations for evaporation in vacuum (*11*, *12*, *20*, *22*), which is most likely due to partial equilibration between chondrule melt and vapor at high temperature (*11*, *12*, *47*, *48*, *52*–*56*).

The light K and Rb isotopic compositions of the chondrule component relative to the CI-like matrix cannot be explained by equilibrium isotopic fractionation between melt and vapor. At the temperature range relevant to chondrule formation (~1000 to 2000 K), the equilibrium isotopic fractionation between the melt and the vapor, calculated using the force constants reported in (*57*) and using plagioclase as a proxy for melt, is too small (~0.01 to 0.03‰ for Δ^{87}Rb and ~0.03 to 0.09‰ for Δ^{41}K) to explain the observed isotopic fractionation (−0.15‰ for Δ^{87}Rb and −0.37‰ for Δ^{41}K; table S1). Furthermore, the chondrule melt should be enriched in the heavy isotopes under equilibrium, which is opposite to what we observe. Larger isotopic fractionation can be produced at high temperature by evaporation and condensation in kinetic regimes when the surrounding vapor medium is either undersaturated or supersaturated for the

element of interest (*5*–*8*). When the vapor is undersaturated, evaporation can enrich the melt residue in heavy isotopes, which is opposite to what is observed here. Conversely, when the surrounding vapor medium is supersaturated, condensation can enrich the melt in the light isotopes, which is consistent with the observed chondrule-matrix fractionation. During fast cooling, the equilibrium vapor pressure decreases rapidly, giving rise to oversaturation and condensation in a kinetic regime. The light MVE isotopic composition of chondrules can therefore be a natural consequence of chondrule cooling.

Isotopic constraints on the overall cooling rate of chondrules

In this section, we test quantitatively whether condensation can explain the MVE depletion and isotopic fractionation in the chondrule component, by relating the observed isotopic fractionations to chondrule cooling rates. The expectation is that, if condensation is the main culprit, the calculated chondrule cooling rate based on MVE isotopes should be consistent with the cooling rates obtained from independent constraints.

Isotopic fractionation during condensation is very sensitive to cooling rates/time scales (*7*, *58*). The magnitude of isotopic fractionation of an element between vapor and melt during partial condensation depends largely on the saturation level of the element in the vapor ($S = P/P_{eq}$; the partial pressure of an element divided by its equilibrium vapor pressure). The larger the degree of supersaturation is, the more fractionated condensing atoms are relative to the vapor. At infinite supersaturation ($S \rightarrow \infty$), the instantaneous isotopic fractionation between the condensate and the vapor is given approximately by the square root of the masses of the isotopes, $\Delta^{i/j}_{Kin} = 1000(\sqrt{m_j/m_i} - 1)$, corresponding to values of −25 and −12‰ for $^{41}K/^{39}K$ and $^{87}Rb/^{85}Rb$ ratios, respectively. At finite supersaturation, the instantaneous isotopic fractionation between the condensing flux (c) and the vapor (v) is $\delta^{i/j}_c - \delta^{i/j}_v \simeq (1 - 1/S)\Delta^{i/j}_{Kin}$ (*7*, *8*), and the degree of supersaturation ($S = P/P_{eq}$) will depend on the cooling rate. As the system cools, the equilibrium vapor pressure decreases, and the partial vapor pressure adjusts to this change through condensation. If the pace of cooling is faster than the rate of condensation allowed by the kinetic theory of gases (i.e., the rate at which vapor atoms/molecules impinge the chondrule surface and stick to it), then the vapor will become supersaturated. Conversely, if the pace of cooling is slow enough, then condensation will be able to bring the vapor pressure to a near-equilibrium state at each instant. Thus, rapid cooling will lead to a high degree of supersaturation and will promote a large kinetic isotopic fractionation between the liquid and the vapor. Slow cooling will allow the vapor and the liquid to remain in near equilibrium during the whole process, resulting in a smaller isotopic fractionation.

Modeling closed-system condensation upon cooling involves calculating equilibrium vapor pressure at each step and computing by how much the vapor pressure decreases at each step because of condensation. Building on the models of isotopic fractionation of the rare earth elements during condensation of refractory inclusions by Hu *et al.* (*58*), we built a simple model to calculate how the chondrule cooling rate influences isotopic fractionation of the chondrule component (see the Supplementary Materials for details). We solved the derived differential equations governing the evolution of the system numerically and tested the validity of the numerical model against analytical equations that we derived for a simplified condensation scenario involving instantaneous cooling (Supplementary Materials and fig. S2). Here, we focus on K and Rb isotopes because (i) K and Rb are less volatile than Zn and Te, and the temperature range at which they condense into chondrules corresponds to the main stage of chondrule melt crystallization (*49*), meaning that the cooling rate estimated based on K and Rb isotopic fractionation should be comparable to the cooling rate based on chondrule textures; (ii) the thermodynamic parameters (Gibbs free energies and activity coefficients) and kinetic parameters (evaporation/condensation coefficients and kinetic isotopic fractionation factors) of Rb and K are better constrained than for Zn and Te at the temperatures relevant to chondrule formation (*54*, *59*–*62*); and (iii) K and Rb are both lithophile elements, meaning that they condense and reside in silicate melt, while Zn and Te are siderophile/chalcophile and their abundances and isotopic fractionations are more easily affected by the presence of metal and sulfide.

Chondrules are classified into types I and II, which differ in their Fe contents and depletions in alkali elements, with type I being more depleted than type II. In general, type I chondrules dominate in CCs, while type II chondrules dominate in ordinary chondrites. Both types are expected to be derived from CI-like starting material (*53*). In our model, we take the CI-like matrix as the bulk initial composition. Assuming that chondrules are evenly distributed in space and form a large and dense cluster, we can examine a single molten chondrule (assuming a typical radius of 0.5 mm) surrounded by a spherical parcel of gas of finite volume (radius $\mathcal{R}$) with no flux boundary conditions at the outer surface (i.e., melt and vapor form a closed system). For calculating the isotopic evolution of the chondrule, the initial state and the cooling path of the chondrule melt-vapor system need to be defined.

The initial state is set with the chondrule heated to a peak temperature of 1550°C (1823 K), corresponding to the value inferred for the most commonly encountered porphyritic chondrules (*63*, *64*). The chondrule is originally in chemical and isotopic equilibrium with the vapor. The vapor pressure and amount of alkali elements in the melt at peak temperature are controlled by the gas radius $\mathcal{R}$. A small $\mathcal{R}$ value corresponds to a high ambient pressure and a large amount of alkali elements in the melt, and vice versa (see the Supplementary Materials and fig. S3). Because $\mathcal{R}$ is unknown, we calculate it by assuming that at peak temperature, half (i.e., 0.24 × CI) of the final amount of K condensed in chondrules (i.e., 0.48 × CI K; table S1) is in the melt, while the rest (0.76 × CI) is in the vapor. This assumption is based on previous work showing that at near-peak temperature, ~50% or less of total condensed Na in type II chondrules was present in the chondrule melt (*48*, *49*). Our study focuses on CCs that contain primarily type I chondrules, which we assume experienced similar alkali volatilization at peak temperature (*50*). In the Supplementary Materials, we also present scenarios in which different amounts of K are present in the chondrule melt at peak temperature (see the Supplementary Materials and figs. S3 and S4). Under the preferred assumption of 0.24 × CI K in the melt at peak temperature, we calculate $\mathcal{R}$ to be 0.069 m (fig. S3), which translates to a chondrule number density of ~727/m^3, in agreement with previous estimates [e.g., (*48*, *54*)]. Under this condition, ~0.1 × CI Rb would be in the chondrule melt, while the rest would be in the vapor at peak temperature (fig. S3). For isotopes, we assume equilibrium between melt and gas at peak temperature, meaning that both K and Rb start with a CI-like isotopic composition in the melt and gas.

During the cooling stage, we assume that temperature decreases linearly with time (i.e., the cooling rate is constant). Cooling leads to oversaturation of alkali elements in the gas associated with kinetic isotopic fractionation. There are two unknowns in the model: the cooling rate and the isolation time/temperature (i.e., the time/temperature

at which chondrule melt stops exchanging with the vapor). The fact that chondrules are depleted in K and Rb relative to CI means that the two elements did not fully recondense into chondrules during cooling, possibly because of the removal of the remaining vapor (or its condensation onto other phases) or abrasion of chondrule surfaces and dust debris removal after condensation. These two unknowns are solved using the two observables (i) condensed fraction and (ii) isotopic composition of an element in chondrules.

In Fig. 4, we plot the isotopic fractionations of Rb and K versus their condensed fractions for different cooling rates (see also fig. S5 for the time evolution of isotopic compositions and condensed fractions). The derived K and Rb isotopic compositions of the chondrule component are consistent with cooling rates of ~900 ± 400 and 470 ± 200 K/hour, respectively (Fig. 4). The large errors associated with the cooling rates, especially for K, arise from uncertainties in both the chemical analyses and the modeling parameters, but this uncertainty is largely inconsequential for using chondrule cooling rate as a constraint on the astrophysical settings responsible for chondrule cooling. The two values agree within error and define a weighted mean of 560 ± 180 K/hour. A larger cooling rate would create larger supersaturation and lead to larger isotopic fractionation for a given condensed fraction, while a lower cooling rate would allow the condensate to exchange further with the vapor, thus limiting the magnitude of isotopic fractionation.

The cooling rate that we calculate is a model value for the chondrule component composition that we derive from the binary mixing model. Chondrules are diverse in size, degree of alkali element depletion, and K isotopic fractionation (*11*, *12*, *20*, *22*). A difficulty with using individual chondrule compositions to constrain cooling rates is that they are more prone to modification by secondary parent body processes such as alteration and metamorphism. For example, solid-state diffusion of K from the matrix to the chondrule could produce light K isotopic composition in the chondrules that could mimic a condensation signature (*65*). With this caveat in mind, we have calculated chondrule cooling rates based on single chondrule data from Allende (*22*). We find cooling rates of ~100 to 2000 K/hour (see the Supplementary Materials and table S2), encompassing the cooling rate derived from the chondrule component. These cooling rates are consistent with those constrained by laboratory experiments trying to reproduce chondrule textures, which yield cooling rates of ~10 to 1000 K/hour for porphyritic chondrules [e.g., (*66*–*68*) and references therein]. Therefore, we conclude that the K and Rb isotopic compositions of chondrules can be well explained by partial condensation of these elements during chondrule cooling, and the isotopic variations measured in bulk CCs are produced by mixing in varying proportions between CI-like matrix and chondrules with fractionated isotopic compositions.

Our study provides a new and independent constraint on the average cooling rate of chondrules in CCs. The cause for the melting of chondrules and their subsequent cooling is still uncertain, but shock waves generated in the solar nebula by planetesimal motion through nebular gas (i.e., planetesimal bow shocks) [e.g., (*69*, *70*)] or by gravitational instability of the nebula (*71*, *72*) provide viable mechanisms to explain the chondrule cooling rate. Alternative models such as the X-wind model (*73*), nebula lightning (*74*, *75*), and shocks induced by the motion of Jupiter (*76*) fail to explain some aspects of the thermal history of chondrules (*68*, *76*). Although the sources of the shock waves are uncertain, larger shocks would be able to produce higher peak temperatures and sustain slower cooling rates than smaller shocks. The overall cooling rate constrained in this study (~560 ± 180 K/hour) would require relatively large shocks. For planetesimal bow shocks, only shocks produced by large planetesimals or planetary embryos (e.g., Mars size) with high velocity (>6 km/s in highly eccentric orbit) can possibly reach the peak temperature of chondrules and, at the same time, sustain the slow cooling rate constrained in this study (*77*). Shock waves induced by gravitational instabilities of the nebula are also consistent with the cooling rate constrained here and are a natural outcome of early protoplanetary disk evolution (*68*, *72*).

MATERIALS AND METHODS

Samples and dissolution

The samples selected for this study (Table 1) are all CC falls, meaning that their residence at Earth's surface was minimal, which helps mitigate the risk of terrestrial contamination or weathering. The

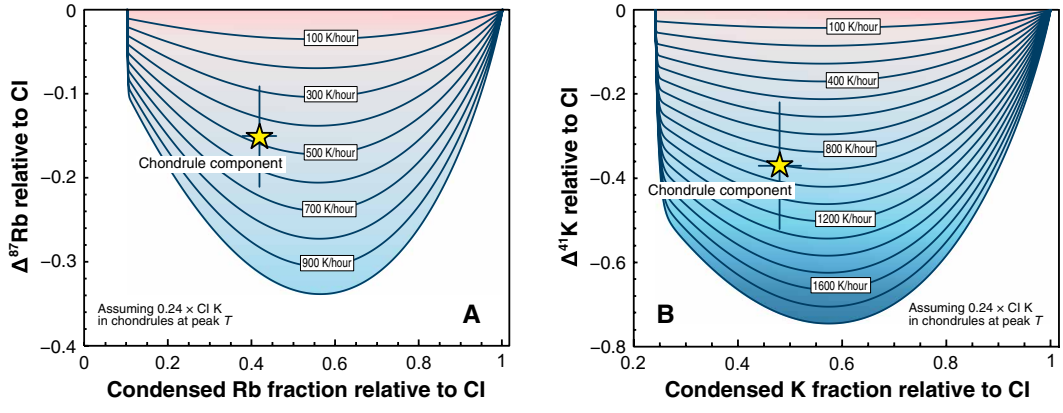

Fig. 4. The model results of condensation during chondrule cooling. Trajectories of Rb (**A**) and K (**B**) isotopic fractionations in chondrules (relative to CI-like matrix; the assumed bulk composition of chondrule and ambient gas) against their condensed fractions are shown (see fig. S5 for the temporal evolution of elemental and isotopic compositions). Gas kinetics imparts light isotopic composition to the condensate, and the degree of isotopic fractionation depends on the degree of supersaturation, which is controlled by the cooling rate. Trajectories are calculated for various cooling rates. Comparing the composition of the chondrule component (yellow stars) with the cooling trajectories (blue curves) yields cooling rates of 470 ± 200 K/hour for Rb (A) and 900 ± 400 K/hour for K (B), with a weighted mean of 560 ± 180 K/hour. This cooling rate agrees with the cooling rate of ~10 to 1000 K/hour constrained from laboratory quenching experiments aimed at reproducing chondrule textures.

samples were obtained in either powder form or as rock chips. The powder aliquots were all homogenized from fragments weighing more than 500 mg. For rock chips, at least 300 mg each was crushed and powdered in a clean agate mortar that is only used for meteorite samples. The powdered samples weighing ~90 to 120 mg each were digested in various mixtures of HF-HNO_3-HCl-$HClO_4$ acids. They were first dissolved at 130°C for at least 24 hours in capped beakers filled with 2:1 volume mixture of concentrated HF-HNO_3 with a few drops of $HClO_4$. The sample solutions were then dried on a hot plate at ~170°C (for evaporating $HClO_4$), then redissolved in aqua regia (3:1 volume mixture of concentrated HCl-HNO_3) in capped beakers at 130°C for another 24 hours. The aqua regia step was repeated a second time. The samples were then dried and redissolved in concentrated HNO_3 and left on the hot plate for another 24 hours. If no residue was visible in the solutions at that point, then the sample solutions were ready for column chromatography. Otherwise, the residue was centrifuged and transferred to a Parr bomb in 3:1 HF-HNO_3 (volume) mixture and heated to ~180°C for at least 3 days for a complete dissolution. The geostandards in this study did not require the Parr bomb step, but the CC samples were all treated with this additional Parr bomb step to ensure complete dissolution. The bombed solutions were then combined with the previously digested solutions for column chromatography. Because K and Rb are highly soluble in acids and the residue amount was in all cases very small, we expect that much of K and Rb was already in solution after hot plate digestion, but the Parr bomb step ensured that even a small amount of K and Rb possibly present in chemically resistant presolar phases was digested. This is important as such presolar grains could be carriers of isotopic anomalies.

Column chromatography for Rb and K purification

After dissolution, 80% of each sample was run through column chromatography to purify Rb and K, and the remaining 20% was stored as spare. The detailed column chemistry procedure used in this study is similar to the method used in (*18*, *78*) and is briefly summarized here. The separation procedure involves four columns: (i) A 16-ml AG 50W-X8 (200 to 400 mesh) cation resin column was used to preconcentrate Na, K, and Rb using 1 M HNO_3 as the sample loading medium and the eluent. (ii) A second 16-ml AG 50W-X8 (200 to 400 mesh) cation resin column was used for eluting K and Rb in 0.5 M HNO_3 to achieve a finer separation. This step separates Rb and K from other elements, but a small amount of Ti can remain. (iii) Titanium was removed from Rb and K by using a 1-ml AG 1-X8 (200 to 400 mesh) anion exchange resin column and 2 M HF as eluent. (iv) Rubidium and potassium were separated from each other using a ~5-ml Sr-Spec resin column (40 cm in length) and 3 M HNO_3 as eluent. This procedure can cleanly isolate both K and Rb, with yields higher than 95% for all samples (yields were also checked for individual columns to ensure a quantitative recovery of K and Rb), and a blank of ~0.14 ng for Rb (the K blank was below the detection level for the MC-ICPMS, corresponding to an upper limit of ~20 ng). The high yields ensure that negligible isotopic fractionation takes place during purification, and the blank contribution is always negligible. The K/Rb weight ratio in CCs is ~250 (Table 1). For MC-ICPMS analysis of Rb, the K/Rb should ideally be less than 10, so as to not affect the accuracy of Rb isotopic measurements (*18*, *78*). Our purification procedure gives a K/Rb ratio lower than 1 in the purified Rb cut. The procedure also efficiently removes Sr ($^{88}Sr/^{85}Rb$ intensity ratio was always <0.0005), so the contribution of ^{87}Sr on ^{87}Rb during MC-ICPMS analysis can be adequately corrected for by assuming a constant $^{87}Sr/^{88}Sr$ ratio of 0.085.

Evaluation of data accuracy

Our measured K isotopic compositions compare well with the K isotopic data reported in (*19*). The long-term (1 year) reproducibility of our K isotopic analysis is ≤0.06‰ (95% c.i.) (*29*). Few high-precision Rb isotope data have been reported. Pringle and Moynier (*17*) reported Rb isotopic data for CCs. Our data overlap with theirs, but some discrepancies exist (fig. S1). Out of all the samples measured, five were measured in both studies: Orgueil, Allende, Vigarano, Murchison, and Lancé. Our measured values are within error of their values for Orgueil, Allende, and Lancé, but the values differ for Murchison and Vigarano (fig. S1). Our $\delta^{87}Rb$ values are +0.12 ± 0.02‰ and +0.06 ± 0.02‰ for Murchison and Vigarano, respectively, while they reported values of +0.02 ± 0.02‰ and −0.10 ± 0.03‰ for the same meteorites. The reason for the discrepancy is unclear, but it could result from sample heterogeneity or from different chemical purification procedures. We therefore developed two different column chromatography methods to test the accuracy of our Rb measurement: the one used in (*18*) that was applied to Rb-depleted lunar samples, and the other that uses only cation resins, similar to that used in (*17*) but with longer columns (*78*).

The second method takes advantage of the unique automated fluoropolymer pneumatic liquid chromatography (FPLC) system developed at the Origins Laboratory of the University of Chicago. Details about this system can be found in (*58*, *78*, *79*, *80*). One of the most important aspects of the FPLC system is that it can use very long and thin columns that require pressurization. The head pressure of the column can be adjusted from ambient pressure to up to 60 psi (~ 4 bar) via high-purity N_2 gas. The elution temperature can also be adjusted from room temperature to 80°C using a water circulation system. The elution is controlled by a software interface and can be run automatically. Sample solutions were first treated using the same column as step (i) outlined above. Rubidium was then purified with the FPLC system using an AG 50W-X12 (200 to 400 mesh) resin. We tested the effects of the column length, temperature, pressure, resin cross-linkage, and acid molarity on the separation of Rb from K and other elements. A clean separation of Rb was achieved with a 130-cm-long, 0.16-cm-wide (inner diameter) column, filled with ~3 ml of AG 50W-X12 resin. Columns were run at room temperature and ~60 psi of pressure. Elution was done using 0.7 M HNO_3. The FPLC method was used to treat Allende and Murchison, two meteorites with large total masses. Our Allende sample is a reference material powder distributed by the Smithsonian Institution. For these two samples, we find the same $\delta^{87}Rb$ values as the values obtained using our standard chromatography method (+0.09 ± 0.02‰ versus +0.08 ± 0.03‰ for Allende; +0.12 ± 0.02‰ versus +0.10 ± 0.02‰ for Murchison; Table 1).

MC-ICPMS analysis

The Rb isotopic compositions of the samples were measured in the Origins Laboratory at the University of Chicago. The measurement method was previously described in (*18*) and is only briefly summarized here. The measurements were done using a Thermo Fisher Scientific Neptune MC-ICPMS upgraded to Neptune Plus specifications in a wet plasma mode. A dual cyclonic-Scott–type quartz spray chamber was used as the sample introduction system, together with normal Ni sampler and skimmer cones, as well as a low-resolution

slit. Standard-sample bracketing was used to correct for instrumental fractionation, with the National Institute of Standards and Technology (NIST) SRM984 as the standard. At least 50 ng of Rb is needed for a precise isotopic analysis, and the amount of Rb purified for each sample was 80 ng or more. Rubidium solutions of 15 to 25 ng/g were introduced into the MC-ICPMS at a flow rate of ~100 μl/min, resulting in a signal intensity of 1.0 to 1.5 V on ^{85}Rb. The isobaric interference ^{87}Sr was subtracted from the ^{87}Rb signal by monitoring ^{88}Sr and assuming an ^{87}Sr/^{88}Sr ratio of 0.085. The ^{88}Sr/^{85}Rb intensity ratio is usually <0.0005, and assuming a slightly different ^{87}Sr/^{88}Sr ratio would not change the result. Isotopic data were collected as a single block of 25 cycles of 4.194-s integration time. Acid blank was measured before and after each sample/standard, and the average was subtracted from the sample/standard signal intensity. Each sample was measured 9 to 12 times, and the average δ^{87}Rb value was calculated. The uncertainty was calculated as the 95% c.i. using the formula of $2\sigma/\sqrt{n}$, with n the number of replicate measurements of a sample and σ the standard deviation of the δ^{87}Rb of the standard bracketed by itself during an entire session (~10 hours, corresponding to ~40 standard-standard brackets). The Student's t factor is not included in our calculation of the uncertainty of the sample mean δ^{87}Rb value because the standard deviation is well characterized from the many repeat analyses of the standard bracketed by itself. All Rb isotopic compositions are reported in δ^{87}Rb notation

$$\delta^{87}\mathrm{Rb} = 1000\left[\left(^{87}\mathrm{Rb}/^{85}\mathrm{Rb}\right)_{\mathrm{Sample}}/\left(^{87}\mathrm{Rb}/^{85}\mathrm{Rb}\right)_{\mathrm{SRM984}} - 1\right]$$

The K isotopic compositions of the samples were measured on a Nu Plasma II MC-ICPMS at the Isotope Laboratory of the University of Washington, Seattle. The main difficulty with K isotope measurements is potential interferences of argon hydrides $^{38}Ar^{1}H^{+}$ and $^{40}Ar^{1}H^{+}$ on $^{39}K^{+}$ and $^{41}K^{+}$. To overcome this problem, K isotopes were measured using a reduced RF forward power "cold plasma," coupled with an Aridus II desolvating nebulizer for sample introduction (*29*). The sample solutions were measured at a concentration of 2 to 3 μg/g K for a signal intensity of 4.5 to 6.5 V on ^{39}K. A high-resolution slit was used to partially resolve the interfering argon hydride peaks, and K isotopes (^{41}K and ^{39}K) were measured on the interference-free peak shoulders. Instrumental mass bias was corrected for using standard-sample bracketing, with NIST SRM3141a as the standard. Each sample analysis consisted of 50 cycles of 4.194-s integration. Acid blank was measured at the beginning of each analytical session and was subtracted from the sample and standard intensities. Each sample was measured five to seven times, and uncertainties were calculated as 95% c.i. using the formula $2\sigma/\sqrt{n}$, with n the number of replicate measurements of a sample and σ the standard deviation of the δ^{41}K of the standard analyzed in the same session bracketed by itself. All K isotopic compositions are reported in δ^{41}K notation

$$\delta^{41}\mathrm{K} = 1000\left[\left(^{41}\mathrm{K}/^{39}\mathrm{K}\right)_{\mathrm{Sample}}/\left(^{41}\mathrm{K}/^{39}\mathrm{K}\right)_{\mathrm{SRM3141a}} - 1\right]$$

SUPPLEMENTARY MATERIALS

Supplementary material for this article is available at https://science.org/doi/10.1126/sciadv.abl3929

REFERENCES AND NOTES

1. E. R. D. Scott, A. N. Krot, Chondrites and their components, in *Meteorites and Cosmochemical Processes*, A. M. Davis, Ed. (Elsevier, Oxford, 2014), vol. 1, pp. 65–137.
2. R. N. Clayton, Oxygen isotopes in meteorites. *Annu. Rev. Earth Planet. Sci.* **21**, 115–149 (1993).
3. N. Dauphas, The isotopic nature of the Earth's accreting material through time. *Nature* **541**, 521–524 (2017).
4. A. M. Davis, Volatile evolution and loss, in *Meteorites and the Early Solar System II*, D. S. Lauretta and H. Y. McSween Jr., Eds. (University of Arizona Press, 2006), pp. 295–307.
5. F. M. Richter, A. M. Davis, D. S. Ebel, A. Hashimoto, Elemental and isotopic fractionation of Type B calcium-, aluminum-rich inclusions: Experiments, theoretical considerations, and constraints on their thermal evolution. *Geochim. Cosmochim. Acta* **66**, 521–540 (2002).
6. F. M. Richter, P. E. Janney, R. A. Mendybaev, A. M. Davis, M. Wadhwa, Elemental and isotopic fractionation of Type B CAI-like liquids by evaporation. *Geochim. Cosmochim. Acta* **71**, 5544–5564 (2007).
7. F. M. Richter, Timescales determining the degree of kinetic isotope fractionation by evaporation and condensation. *Geochim. Cosmochim. Acta* **68**, 4971–4992 (2004).
8. N. Dauphas, F. Poitrasson, C. Burkhardt, H. Kobayashi, K. Kurosawa, Planetary and meteoritic Mg/Si and δ^{30} Si variations inherited from solar nebula chemistry. *Earth Planet. Sci. Lett.* **427**, 236–248 (2015).
9. K. Lodders, Solar system abundances and condensation temperatures of the elements. *Astrophys. J.* **591**, 1220–1247 (2003).
10. F.-Z. Teng, N. Dauphas, J. M. Watkins, Non-traditional stable isotopes: Retrospective and prospective. *Rev. Mineral. Geochem.* **82**, 1–26 (2017).
11. C. M. O. Alexander, J. N. Grossman, J. Wang, B. Zanda, M. Bourot-Denise, R. H. Hewins, The lack of potassium-isotopic fractionation in Bishunpur chondrules. *Meteorit. Planet. Sci.* **35**, 859–868 (2000).
12. C. M. O. Alexander, J. N. Grossman, Alkali elemental and potassium isotopic compositions of Semarkona chondrules. *Meteorit. Planet. Sci.* **40**, 541–556 (2005).
13. K. Wang, S. B. Jacobsen, Potassium isotopic evidence for a high-energy giant impact origin of the Moon. *Nature* **538**, 487–490 (2016).
14. Z. Tian, H. Chen, B. Fegley, K. Lodders, J.-A. Barrat, J. M. D. Day, K. Wang, Potassium isotopic compositions of howardite-eucrite-diogenite meteorites. *Geochim. Cosmochim. Acta* **266**, 611–632 (2019).
15. Z. Tian, B. L. Jolliff, R. L. Korotev, B. Fegley, K. Lodders, J. M. D. Day, H. Chen, K. Wang, Potassium isotopic composition of the Moon. *Geochim. Cosmochim. Acta* **280**, 263–280 (2020).
16. H. Bloom, K. Lodders, H. Chen, C. Zhao, Z. Tian, P. Koefoed, M. K. Pető, Y. Jiang, K. Wang, Potassium isotope compositions of carbonaceous and ordinary chondrites: Implications on the origin of volatile depletion in the early solar system. *Geochim. Cosmochim. Acta* **277**, 111–131 (2020).
17. E. A. Pringle, F. Moynier, Rubidium isotopic composition of the Earth, meteorites, and the Moon: Evidence for the origin of volatile loss during planetary accretion. *Earth Planet. Sci. Lett.* **473**, 62–70 (2017).
18. N. X. Nie, N. Dauphas, Vapor drainage in the protolunar disk as the cause for the depletion in volatile elements of the moon. *Astrophys. J. Lett.* **884**, L48 (2019).
19. Y. Ku, S. B. Jacobsen, Potassium isotope anomalies in meteorites inherited from the protosolar molecular cloud. *Sci. Adv.* **6**, eabd0511 (2020).
20. P. Koefoed, O. Pravdivtseva, H. Chen, C. Gerritzen, M. M. Thiemens, K. Wang, Potassium isotope systematics of the LL4 chondrite Hamlet: Implications for chondrule formation and alteration. *Meteorit. Planet. Sci.* **55**, (2020).
21. C. Zhao, K. Lodders, H. Bloom, H. Chen, Z. Tian, P. Koefoed, M. K. Pető, K. Wang, Potassium isotopic compositions of enstatite meteorites. *Meteorit. Planet. Sci.* **55**, 1404–1417 (2020).
22. Y. Jiang, P. Koefoed, O. Pravdivtseva, H. Chen, C.-H. Li, F. Huang, L.-P. Qin, J. Liu, K. Wang, Early solar system aqueous activity: K isotope evidence from Allende. *Meteorit. Planet. Sci.* **56**, 61–76 (2021).
23. J. L. Hellmann, T. Hopp, C. Burkhardt, T. Kleine, Origin of volatile element depletion among carbonaceous chondrites. *Earth Planet. Sci. Lett.* **549**, 116508 (2020).
24. J.-M. Luck, D. B. Othman, F. Albarède, Zn and Cu isotopic variations in chondrites and iron meteorites: Early solar nebula reservoirs and parent-body processes. *Geochim. Cosmochim. Acta* **69**, 5351–5363 (2005).
25. E. A. Pringle, F. Moynier, P. Beck, R. Paniello, D. C. Hezel, The origin of volatile element depletion in early solar system material: Clues from Zn isotopes in chondrules. *Earth Planet. Sci. Lett.* **468**, 62–71 (2017).
26. C. M. O. Alexander, Quantitative models for the elemental and isotopic fractionations in chondrites: The carbonaceous chondrites. *Geochim. Cosmochim. Acta* **254**, 277–309 (2019).
27. D. Clayton, *Handbook of Isotopes in the Cosmos: Hydrogen to Gallium* (Cambridge Univ. Press, 2007).
28. E. Anders, N. Grevesse, Abundances of the elements: Meteoritic and solar. *Geochim. Cosmochim. Acta* **53**, 197–214 (1989).
29. Y. Hu, X.-Y. Chen, Y.-K. Xu, F.-Z. Teng, High-precision analysis of potassium isotopes by HR-MC-ICPMS. *Chem. Geol.* **493**, 100–108 (2018).
30. M. A. Fehr, S. J. Hammond, I. J. Parkinson, Tellurium stable isotope fractionation in chondritic meteorites and some terrestrial samples. *Geochim. Cosmochim. Acta* **222**, 17–33 (2018).

31. A. N. Krot, E. R. D. Scott, M. E. Zolensky, Mineralogical and chemical modification of components in CV3 chondrites: Nebular or asteroidal processing? *Meteoritics* **30**, 748–775 (1995).
32. A. Hashimoto, L. Grossman, Alteration of Al-rich inclusions inside amoeboid olivine aggregates in the Allende meteorite. *Geochim. Cosmochim. Acta* **51**, 1685–1704 (1987).
33. E. Anders, Origin, age, and composition of meteorites. *Space Sci. Rev.* **3**, 583–714 (1964).
34. J. W. Larimer, E. Anders, Chemical fractionations in meteorites—II. Abundance patterns and their interpretation. *Geochim. Cosmochim. Acta* **31**, 1239–1270 (1967).
35. F. Wlotzka, H. Palme, B. Spettel, H. Wänke, K. Fredriksson, A. F. Noonan, Alkali differentiation in LL-chondrites. *Geochim. Cosmochim. Acta* **47**, 743–757 (1983).
36. T. Yokoyama, K. Misawa, O. Okano, C.-Y. Shih, L. E. Nyquist, J. I. Simon, M. J. Tappa, S. Yoneda, Extreme early solar system chemical fractionation recorded by alkali-rich clasts contained in ordinary chondrite breccias. *Earth Planet. Sci. Lett.* **458**, 233–240 (2017).
37. L. H. Fuchs, Djerfisherite, alkali copper-iron sulfide: A new mineral from enstatite chondrites. *Science* **153**, 166–167 (1966).
38. J. L. Hellmann, T. Hopp, C. Burkhardt, H. Becker, M. Fischer-Gödde, T. Kleine, Tellurium isotope cosmochemistry: Implications for volatile fractionation in chondrite parent bodies and origin of the late veneer. *Geochim. Cosmochim. Acta* **309**, 313–328 (2021).
39. F. Wombacher, M. Rehkämper, K. Mezger, A. Bischoff, C. Münker, Cadmium stable isotope cosmochemistry. *Geochim. Cosmochim. Acta* **72**, 646–667 (2008).
40. M. Schönbächler, R. W. Carlson, M. F. Horan, T. D. Mock, E. H. Hauri, Silver isotope variations in chondrites: Volatile depletion and the initial 107Pd abundance of the solar system. *Geochim. Cosmochim. Acta* **72**, 5330–5341 (2008).
41. H. Palme, D. C. Hezel, D. S. Ebel, The origin of chondrules: Constraints from matrix composition and matrix-chondrule complementarity. *Earth Planet. Sci. Lett.* **411**, 11–19 (2015).
42. D. C. Hezel, H. Palme, The chemical relationship between chondrules and matrix and the chondrule matrix complementarity. *Earth Planet. Sci. Lett.* **294**, 85–93 (2010).
43. B. Zanda, M. Humayun, R. Hewins, Chemical composition of matrix and chondrules in carbonaceous chondrites: Implications for disk transport, in *Proceedings of the 43rd Annual Lunar and Planetary Science Conference*, Woodlands, TX, USA (19 to 23 March 2012), p. 2413.
44. E. M. M. E. van Kooten, F. Moynier, A. Agranier, A unifying model for the accretion of chondrules and matrix. *Proc. Natl. Acad. Sci. U.S.A.* **116**, 18860–18866 (2019).
45. E. van Kooten, F. Moynier, Zinc isotope analyses of singularly small samples (<5 ng Zn): Investigating chondrule-matrix complementarity in Leoville. *Geochim. Cosmochim. Acta* **261**, 248–268 (2019).
46. G. Libourel, A. N. Krot, L. Tissandier, Role of gas-melt interaction during chondrule formation. *Earth Planet. Sci. Lett.* **251**, 232–240 (2006).
47. G. Libourel, M. Portail, Chondrules as direct thermochemical sensors of solar protoplanetary disk gas. *Sci. Adv.* **4**, eaar3321 (2018).
48. C. M. O. Alexander, J. N. Grossman, D. S. Ebel, F. J. Ciesla, The formation conditions of chondrules and chondrites. *Science* **320**, 1617–1619 (2008).
49. R. H. Hewins, B. Zanda, C. Bendersky, Evaporation and recondensation of sodium in Semarkona Type II chondrules. *Geochim. Cosmochim. Acta* **78**, 1–17 (2012).
50. L. Florentin, F. Faure, E. Deloule, L. Tissandier, A. Gurenko, D. Lequin, Origin of Na in glass inclusions hosted in olivine from Allende CV3 and Jbilet Winselwan CM2: Implications for chondrule formation. *Earth Planet. Sci. Lett.* **474**, 160–171 (2017).
51. G. Libourel, A. Krot, L. Tissandier, Evidence for high temperature condensation of moderately-volatile elements during chondrule formation, in *Proceedings of the 34th Annual Lunar and Planetary Science Conference*, League City, TX, USA (17 to 21 March 2003), p. 1558.
52. R. D. Lewis, G. E. Lofgren, H. F. Franzen, K. E. Windom, The effect of Na vapor on the Na content of chondrules. *Meteoritics* **28**, 622–628 (1993).
53. B. A. Cohen, R. H. Hewins, C. M. O. Alexander, The formation of chondrules by open-system melting of nebular condensates. *Geochim. Cosmochim. Acta* **68**, 1661–1675 (2004).
54. F. M. Richter, R. A. Mendybaev, J. N. Christensen, D. Ebel, A. Gaffney, Laboratory experiments bearing on the origin and evolution of olivine-rich chondrules. *Meteorit. Planet. Sci.* **46**, 1152–1178 (2011).
55. A. V. Fedkin, L. Grossman, Vapor saturation of sodium: Key to unlocking the origin of chondrules. *Geochim. Cosmochim. Acta* **112**, 226–250 (2013).
56. P. Georges, G. Libourel, E. Deloule, Experimental constraints on alkali condensation in chondrule formation. *Meteorit. Planet. Sci.* **35**, 1183–1188 (2000).
57. H. Zeng, V. F. Rozsa, N. X. Nie, Z. Zhang, T. A. Pham, G. Galli, N. Dauphas, Ab initio calculation of equilibrium isotopic fractionations of potassium and rubidium in minerals and water. *ACS Earth Space Chem.* **3**, 2601–2612 (2019).
58. J. Y. Hu, N. Dauphas, F. L. H. Tissot, R. Yokochi, T. J. Ireland, Z. Zhang, A. M. Davis, F. J. Ciesla, L. Grossman, B. L. A. Charlier, M. Roskosz, E. E. Alp, M. Y. Hu, J. Zhao, Heating events in the nascent solar system recorded by rare earth element isotopic fractionation in refractory inclusions. *Sci. Adv.* **7**, eabc2962 (2021).
59. Y. Yu, R. H. Hewins, C. M. O. Alexander, J. Wang, Experimental study of evaporation and isotopic mass fractionation of potassium in silicate melts. *Geochim. Cosmochim. Acta* **67**, 773–786 (2003).
60. A. V. Fedkin, L. Grossman, M. S. Ghiorso, Vapor pressures and evaporation coefficients for melts of ferromagnesian chondrule-like compositions. *Geochim. Cosmochim. Acta* **70**, 206–223 (2006).
61. P. A. Sossi, S. Klemme, H. S. C. O'Neill, J. Berndt, F. Moynier, Evaporation of moderately volatile elements from silicate melts: Experiments and theory. *Geochim. Cosmochim. Acta* **260**, 204–231 (2019).
62. Z. J. Zhang, N. X. Nie, R. A. Mendybaev, M.-C. Liu, J. J. Hu, T. Hopp, E. E. Alp, B. Lavina, E. S. Bullock, K. D. McKeegan, Loss and isotopic fractionation of alkali elements during diffusion-limited evaporation from molten silicate: Theory and experiments. *ACS Earth Space Chem.* **5**, 755–784 (2021).
63. R. H. Hewins, H. C. Connolly Jr., Peak temperatures of flash-melted chondrules, in *Proceedings of the International conference: Chondrules and the Protoplanetary Disk* (1996), pp. 197–204.
64. R. H. Hewins, P. M. Radomsky, Temperature conditions for chondrule formation. *Meteoritics* **25**, 309–318 (1990).
65. F. M. Richter, N. Dauphas, F.-Z. Teng, Non-traditional fractionation of non-traditional isotopes: Evaporation, chemical diffusion and Soret diffusion. *Chem. Geol.* **258**, 92–103 (2009).
66. G. Lofgren, W. J. Russell, Dynamic crystallization of chondrule melts of porphyritic and radial pyroxene composition. *Geochim. Cosmochim. Acta* **50**, 1715–1726 (1986).
67. P. M. Radomsky, R. H. Hewins, Formation conditions of pyroxene-olivine and magnesian olivine chondrules. *Geochim. Cosmochim. Acta* **54**, 3475–3490 (1990).
68. S. J. Desch, M. A. Morris, H. C. Connolly, A. P. Boss, The importance of experiments: Constraints on chondrule formation models. *Meteorit. Planet. Sci.* **47**, 1139–1156 (2012).
69. L. L. Hood, Thermal processing of chondrule precursors in planetesimal bow shocks. *Meteorit. Planet Sci.* **33**, 97–107 (1998).
70. F. J. Ciesla, L. L. Hood, S. J. Weidenschilling, Evaluating planetesimal bow shocks as sites for chondrule formation. *Meteorit. Planet Sci.* **39**, 1809–1821 (2004).
71. J. A. Wood, Processing of chondritic and planetary material in spiral density waves in the nebula. *Meteorit. Planet Sci.* **31**, 641–645 (1996).
72. A. P. Boss, R. H. Durisen, Chondrule-forming shock fronts in the solar nebula: A possible unified scenario for planet and chondrite formation. *Astrophys. J.* **621**, L137–L140 (2005).
73. F. H. Shu, H. Shang, T. Lee, Toward an astrophysical theory of chondrites. *Science* **271**, 1545–1552 (1996).
74. W. Pilipp, T. W. Hartquist, G. E. Morfill, E. Levy, Chondrule formation by lightning in the Protosolar Nebula? *Astron. Astrophys.* **331**, 121–146 (1998).
75. S. J. Desch, J. N. Cuzzi, The generation of lightning in the solar nebula. *Icarus* **143**, 87–105 (2000).
76. J.-D. Bodénan, C. Surville, J. Szulágyi, L. Mayer, M. Schönbächler, Can chondrules be produced by the interaction of Jupiter with the protosolar disk? *Astrophys. J.* **901**, 60 (2020).
77. C. R. Mann, A. C. Boley, M. A. Morris, Planetary embryo bow shocks as a mechanism for chondrule formation. *Astrophys. J.* **818**, 103 (2016).
78. N. X. Nie, N. Dauphas, T. Hopp, J.-Y. Hu, Z. J. Zhang, R. Yokochi, T. Ireland, F. L. Tissot, Chromatography purification of Rb for accurate isotopic analysis by MC-ICPMS: a comparison between AMP-PAN, cation-exchange, and Sr resins. *J. Anal. At. Spectrom.* (2021).
79. T. J. Ireland, F. L. H. Tissot, R. Yokochi, N. Dauphas, Teflon-HPLC: A novel chromatographic system for application to isotope geochemistry and other industries. *Chem. Geol.* **357**, 203–214 (2013).
80. N. Dauphas, F. L. H. Tissot, R. Yokochi, T. J. Ireland, U.S. Patent US20150008171A1 (2015); https://patents.google.com/patent/US20150008171A1/en.
81. A. V. Fedkin, L. Grossman, F. J. Ciesla, S. B. Simon, Mineralogical and isotopic constraints on chondrule formation from shock wave thermal histories. *Geochim. Cosmochim. Acta* **87**, 81–116 (2012).
82. J. M. Friedrich, M. K. Weisberg, D. S. Ebel, A. E. Biltz, B. M. Corbett, I. V. Iotzov, W. S. Khan, M. D. Wolman, Chondrule size and related physical properties: A compilation and evaluation of current data across all meteorite groups. *Geochemistry* **75**, 419–443 (2015).
83. J. L. Gooding, K. Keil, Relative abundances of chondrule primary textural types in ordinary chondrites and their bearing on conditions of chondrule formation. *Meteoritics* **16**, 17–43 (1981).
84. C. M. O. Alexander, D. S. Ebel, Questions, questions: Can the contradictions between the petrologic, isotopic, thermodynamic, and astrophysical constraints on chondrule formation be resolved? *Meteorit. Planet Sci.* **47**, 1157–1175 (2012).
85. B. R. Frost, Introduction to oxygen fugacity and its petrologic importance, in *Oxide Minerals* (De Gruyter, 2018), pp. 1–10.

86. B. Bourdon, C. Fitoussi, Isotope fractionation during condensation and evaporation during planet formation processes. *ACS Earth Space Chem.* **4**, 1408–1423 (2020).
87. H. Y. McSween Jr., Chemical and petrographic constraints on the origin of chondrules and inclusions in carbonaceous chondrites. *Geochim. Cosmochim. Acta* **41**, 1843–1860 (1977).
88. J. T. Wasson, G. W. Kallemeyn, Compositions of chondrites. *Philos. Trans. R. Soc., A* **325**, 535–544 (1988).
89. R. H. Hewins, M. Bourot-Denise, B. Zanda, H. Leroux, J.-A. Barrat, M. Humayun, C. Göpel, R. C. Greenwood, I. A. Franchi, S. Pont, J.-P. Lorand, C. Cournède, J. Gattacceca, P. Rochette, M. Kuga, Y. Marrocchi, B. Marty, The Paris meteorite, the least altered CM chondrite so far. *Geochim. Cosmochim. Acta* **124**, 190–222 (2014).
90. H. Y. McSween, Alteration in CM carbonaceous chondrites inferred from modal and chemical variations in matrix. *Geochim. Cosmochim. Acta* **43**, 1761–1770 (1979).
91. H. Y. McSween Jr., Carbonaceous chondrites of the Ornans type: A metamorphic sequence. *Geochim. Cosmochim. Acta* **41**, 477–491 (1977).
92. H. Y. Mcsween Jr., Petrographic variations among carbonaceous chondrites of the Vigarano type. *Geochim. Cosmochim. Acta* **41**, 1777–1790 (1977).
93. J. Bayron, I. Erb, D. Ebel, S. Wallace, H. Connolly, Modal abundances and chemistry of clasts in the Renazzo (CR2) chondrite by x-ray map analysis, in *Proceedings of the 45th Annual Lunar and Planetary Science Conference*, Woodlands, TX, USA (17 to 21 March 2014), p. 1225.
94. D. L. Schrader, I. A. Franchi, H. C. Connolly Jr., R. C. Greenwood, D. S. Lauretta, J. M. Gibson, The formation and alteration of the Renazzo-like carbonaceous chondrites I: Implications of bulk-oxygen isotopic composition. *Geochim. Cosmochim. Acta* **75**, 308–325 (2011).
95. A. I. Blinova, T. J. Zega, C. D. K. Herd, R. M. Stroud, Testing variations within the Tagish Lake meteorite—I: Mineralogy and petrology of pristine samples. *Meteorit. Planet Sci.* **49**, 473–502 (2014).

Acknowledgments: Discussions with C. M. O. Alexander were greatly appreciated. Constructive comments from H. Palme and an anonymous reviewer helped improve the quality of the manuscript and were very much appreciated. We thank P. Heck, the Robert A. Pritzker Center for Meteoritics and Polar Studies of the Field Museum, and the Muséum National d'Histoire Naturelle for providing the meteorite samples analyzed in this study. **Funding:** This work was supported by a NASA NESSF fellowship (NNX15AQ97H), a Carnegie postdoctoral fellowship, and a Carnegie Postdoc × Postdoc (P^2) seed grant to N.X.N., NASA grants NNX17AE86G (LARS), NNX17AE87G (EW), 80NSSC17K0744 (HW), 80NSSC21K0380 (EW), 80NSSC20K0821 (EW), 80NSSC20K1409 (SSW), and NSF grant EAR-2001098 (CSEDI) to N.D. **Author contributions:** N.X.N. and N.D. conceived the study. N.X.N. performed the digestion and chromatographic purification of Rb and K from the samples. N.X.N. and X.-Y.C. carried out the isotopic analyses of Rb and K by MC-ICPMS. N.X.N., N.D., J.Y.H., and Z.J.Z. did the modeling. T.H., A.S., and F.-Z.T. helped with data interpretation. N.X.N., N.D., and T.H. wrote the manuscript, which was edited by all the other authors. **Competing interests:** The authors declare that they have no competing interests. **Data and materials availability:** All data needed to evaluate the conclusions in the paper are present in the paper and/or the Supplementary Materials.

Submitted 12 July 2021
Accepted 14 October 2021
Published 1 December 2021
10.1126/sciadv.abl3929